ACS Photonics

Article

pubs.acs.org/journal/apchd5

Effect of Threading Dislocations on the Quality Factor of InGaN/GaN Microdisk Cavities

Tim J. Puchtler,*[,†] Alexander Woolf,[‡] Tongtong Zhu,[†] David Gachet,[§] Evelyn L. Hu,[‡] and Rachel A. Oliver[†]

[†]Department of Materials Science and Metallurgy, University of Cambridge, 27 Charles Babbage Road, Cambridge, CB3 0FS, U.K.

[‡]School of Engineering and Applied Science, Harvard University, Cambridge, Massachusetts 02138, United States

[§]Attolight AG, EPFL Innovation Park - Bâtiment D, CH-1015 Lausanne, Switzerland

ABSTRACT: In spite of the theoretical advantages associated with nitride microcavities, the quality factors of devices with embedded indium gallium nitride (InGaN) or gallium nitride (GaN) optical emitters still remain low. In this work we identify threading dislocations (TDs) as a major limitation to the fabrication of high quality factor devices in the nitrides. We report on the use of cathodoluminescence (CL) to identify individual TD positions within microdisk lasers containing either InGaN quantum wells or quantum dots. Using CL to accurately count the number, and map the position, of dislocations within several individual cavities, we have found a clear correlation between the density of defects in the high-field region of a microdisk and its corresponding quality factor (Q). We discuss possible mechanisms associated with defects, photon scattering, and absorption, which could be responsible for degraded device performance.

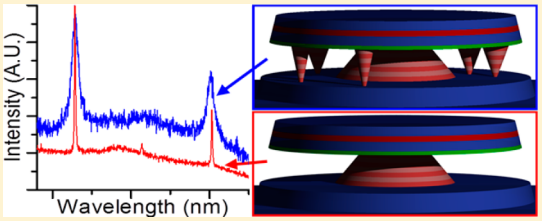

KEYWORDS: *threading dislocations, gan, quality factor, microcavities, cathodoluminescence*

GaN microcavities with embedded optical emitters have long been sought after as visible light sources as well as platforms for cavity quantum electrodynamics (cQED). Inherent advantages of nitride-based microcavities include low surface recombination velocities,[1] enhanced room-temperature performance due to their high exciton binding energy (from 20 meV in bulk GaN to ∼36 meV for QDs),[2,3] and emission wavelengths in the blue region of the visible spectrum.[4] Recent progress with InGaN optical emitters include strong coupling and polariton lasing in microcavities featuring distributed Bragg reflectors (DRBs),[5] low threshold lasing,[6] observations of Rabi oscillations,[7] and single-photon emission.[8] However, in spite of such progress the quality factors in the nitrides are often more than an order of magnitude lower than other III−V systems.[9−11] This, as well as the large joint density of states of InGaN/GaN devices, causes lasing thresholds to be significantly higher than for other III−V systems.[12,13]

While the GaN materials system is notable for both strong internal fields and dislocation densities, which would be expected to destroy device performance in other material systems,[14] the performance of some nitride devices such as light-emitting diodes and HEMTs is excellent and does not appear to be limited by the high defect density. The mechanisms by which devices are robust to dislocations are still debated.[15] In previous work, statistical analysis of a score of microdisk devices found an anticorrelation between the quality factor (Q) of those devices and the overall dislocation density of the material composing the sample. However, the reasons underlying that anticorrelation were not fully discussed, nor were the dislocation densities of individual disks measured.[16] Here we expand upon such work by the novel exploitation of cathodoluminescence (CL) techniques to help make correlations between the locations of threading dislocations (TDs) in individual microdisks with the Q of that specific device, allowing unprecedented understanding of the effect of TDs in these devices.

A schematic of the device is shown in Figure 1. The microdisk membrane has a thickness of 200 nm and encapsulates three layers of 2.5 nm thick $In_xGa_{1-x}N$ quantum wells (QWs) or quantum dots (QDs), with each layer in the latter case having an approximate areal density of QDs of 10^{10} cm^{-2} and QD height of 1.2 ± 0.1 nm based on atomic force

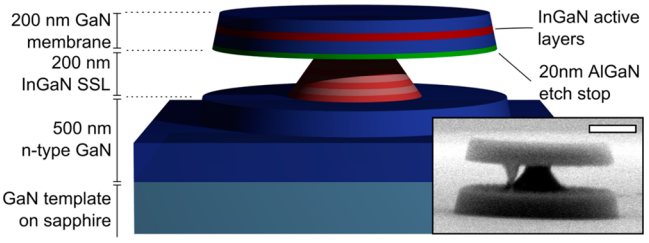

Figure 1. Schematic of GaN microdisk with its respective epilayers. The suspended disk membrane has a thickness of 200 nm and diameter of 1.2 μm, containing either three QD or QW active layers. (Inset) Scanning electron microscope (SEM) image of a completed microdisk from the side. Scale bar represents 400 nm.

Received: September 26, 2014
Published: December 17, 2014

DOI: 10.1021/ph500426g
ACS Photonics 2015, 2, 137−143

microscopy (AFM) studies of QD epilayers grown contemporaneously. A disk radius of 1 μm has been chosen in order to create the smallest possible modal volume without a negative impact on quality factor; the low modal volume is significant to both lasing and coupling enhancement applications of the microdisks. The composition, x, of the $In_xGa_{1-x}N$ was approximately 0.2. A 200 nm $In_yGa_{1-y}N/In_zGa_{1-z}N$ sacrificial superlattice (SSL, y = 5.0%, z = 6.5% In) serves as the pedestal for the disk membrane, which was capped by a thin (~10 nm) GaN layer, followed by a 20 nm $Al_{0.2}Ga_{0.8}N$ etch stop layer. These structures were grown atop n-doped c-plane GaN/Al_2O_3 pseudosubstrates, which have been deliberately grown to achieve different densities of threading dislocations (3.0×10^8, 5.6×10^8, and 5.3×10^9 cm^{-2}) measured by AFM scans of silane-treated pseudosubstrates.[17] Microdisk cavities were formed concurrently from each sample using techniques that have been previously described.[18,19] A photoelectrochemical (PEC) etch was employed to remove the outer region of the sacrificial superlattice and thus undercut the disk membrane, allowing for enhanced optical confinement in the vertical dimension.

Six samples with differing InGaN active regions were investigated, separated into two sets: three samples contained QDs formed by "droplet epitaxy" grown on pseudosubstrates of varying dislocation density;[20,21] and three QW samples with differing growth conditions were grown on low-dislocation templates (approximate density $(3.0 \pm 0.3) \times 10^8$ cm^{-2}). The QW samples were selected to investigate whether InGaN quantity or defect inclusion would affect cavity quality factors, consisting of QWs with GaN capping layers grown at a single temperature (740 °C); capping layers that were temperature ramped during growth (725–860 °C) to reduce defect incorporation; and a postgrowth NH_3 anneal, causing fragmented QWs (fQWs). A Student's t-test comparing the mean quality factors of the different QW samples suggests that there is no statistically significant effect (p = 0.78) of the different growth treatments on the analysis presented in this work. Further analysis of the impact of the different active layers on microdisk performance will be discussed elsewhere.[22]

OBSERVATION OF DISLOCATIONS

Microdisk resonators were investigated using separate microphotoluminescence (μPL) and cathodoluminescence setups. Markers on the fabricated samples were used to identify the same disk in both setups, allowing disks measured in μPL to be subsequently imaged by SEM-CL (Figure 2). Threading dislocations act as nonradiative recombination centers, and hence emission from the QWs in their vicinity is reduced.[23] This causes the appearance of dark spots in the CL images (Figure 2a), allowing the number and position of individual dislocations to be recorded for each microdisk examined. It should be noted that there may be other causes of dark spots in CL imaging, such as dirt and InGaN composition fluctuations in QD samples. Careful sample preparation, consistent imaging conditions, and plasma cleaning of samples reduce the incidence of misidentification of dislocations, although may not eliminate it completely. The spatial resolution of the CL images is dependent on both the size of the interaction volume and the diffusion length of carriers in the material. While the spot size may be measured, the diffusion length is not well known. Nonetheless, comparison of AFM and CL data on similar samples indicates that CL is well able to resolve individual dislocations in materials of the dislocation density used here.

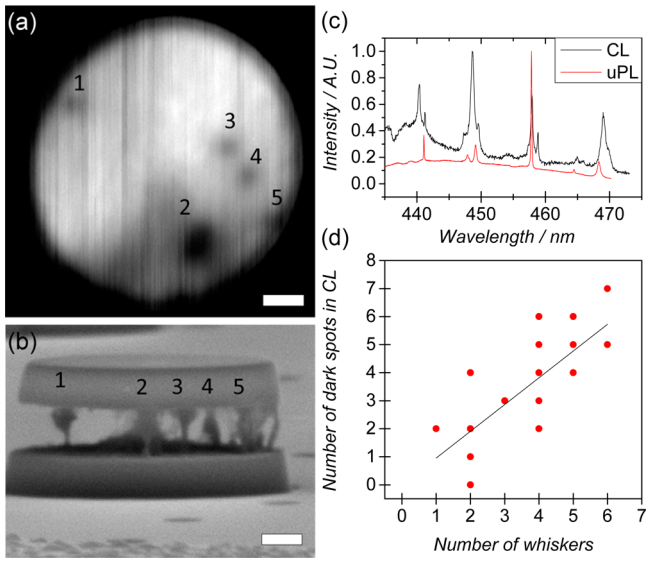

Figure 2. (a) Example plan-view CL and (b) corresponding side-view SEM images of a highly undercut microdisk. Dark spots in CL are attributed to dislocations and have had their positions marked. The central pillar is visible behind dislocation 2. Note that dislocation size can vary significantly. Scale bar represents 200 nm. (c) Overlaid μPL and CL spectra obtained from the same microdisk at room temperature showing WGM peaks. (d) Relationship between number of dark spots counted in CL and number of whiskers counted in SEM for 18 samples (several data points are superimposed). This has been fitted to $y = mx$, giving a value of m = 0.94, with R^2 = 0.5.

The presence of dislocations also leads to deformations referred to as "whiskers", which decorate the underside of the cavity, as can be seen in Figure 2b.[24] The whiskers arise from the PEC etch technique, which is employed to undercut the cavity membrane; the threading dislocations act as charge trapping sites, which inhibit photogenerated electron–hole pair separation and subsequent removal of the sacrificial region around the defect.[25] The number of whiskers and dark spots in CL has been counted for a range of disks in order to assess the strength of correlation between the presence of a dislocation and formation of a whisker. The relationship appears linear, giving a best fit with gradient of 0.94 and an R^2 of 0.53 (Figure 2d).

Q-factors were extracted from modal peaks in PL, with the microdisk Q given as the maximum Q obtained from any mode. The CL spectra confirmed the frequency values of the whispering gallery modes (WGMs); however the measured quality factors were systematically lower than corresponding PL results. Such a discrepancy is expected, due to both the carbon contamination deposited on the sample surface from the electron beam and the increased spectral jitter due to the changing electronic environment in the disk as the beam position is rastered across the surface. Therefore, the Q values reported in this work were obtained using PL.

As expected, finite-difference time-domain (FDTD) simulations of a 1.2 μm GaN microdisk cavity suggest that the highest Q modes, the WGMs, are confined to the periphery of the disk membrane (Figure 3a). To confirm that this modal pattern exists in the fabricated cavities, CL emission spectra were taken at each beam position during SEM imaging of a disk. The hyperspectral image created contains the emission

DOI: 10.1021/ph500426g
ACS Photonics 2015, 2, 137–143

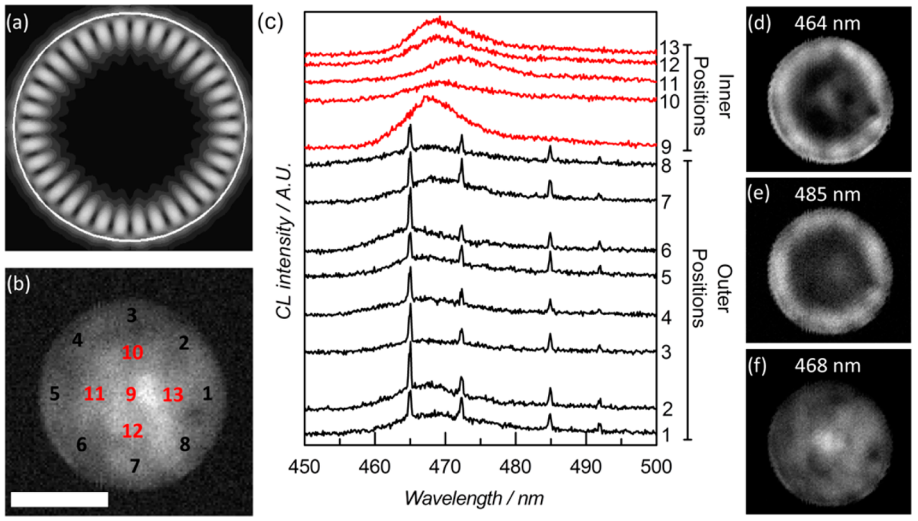

Figure 3. (a) FDTD simulation of a first-order WGM in a 1.2 μm diameter GaN microdisk, showing high intensity in the outer 200 nm of the cavity. (b) Panchromatic intensity map of an imaged QW disk taken with the Attolight CL system operating with 3 kV at 15 K. Scale bar represents 500 nm. Several positions have been marked, with (c) corresponding to CL spectra in which we can see WGM peaks in all positions at the periphery of the disk, but only background emission when imaging the center of the disk. Example monochromatic CL images taken at WGM wavelengths, (d) 464 nm and (e) 485 nm, show the greatest optical intensity when scanning in the WGM volume, validating the FDTD shown in (a). By comparison an image taken at a typical background wavelength of 468 nm (f) shows near-uniform emission across the disk.

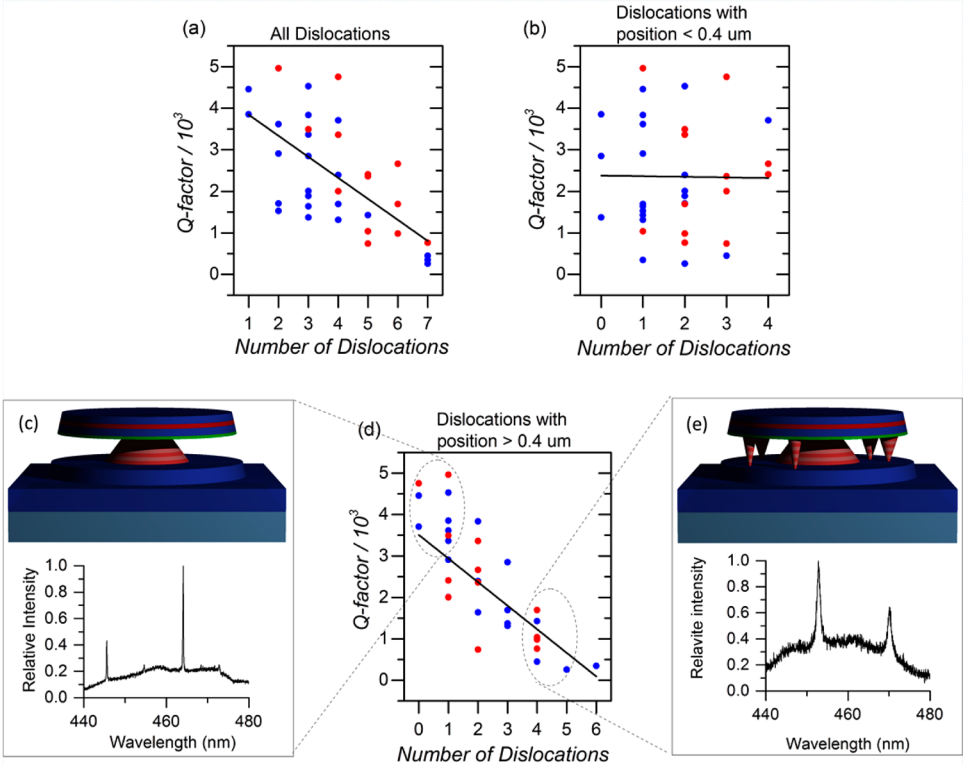

Figure 4. Graphs of microdisk Q vs number of threading dislocations with radial position (a) 0–0.6 μm, (b) <0.4 μm, and (d) >0.4 μm for (red) QW- and (blue) QD-containing microdisks. Linear fits to this data give R^2 values of 0.42, 0.0001, and 0.47, respectively. A schematic of, and representative μPL spectrum taken from, microdisks of both (c) low and (e) high dislocation numbers in the periphery of the disks.

spectra of the disk for each position of e-beam excitation and hence allows comparison of the spectra caused by excitation in the periphery of the disk relative to those excited at the center (Figure 3b,c). Images suggest that first-order WGMs are located at positions greater than 0.4 μm from the center of the disk, consistent with the results of the model. We define this part of the disk as the "outer region" and contrast it with the inner region (material less than 0.4 μm from the center of the disk) in the analysis below.

IMPACT OF DISLOCATIONS ON CAVITY Q

Using the CL-imaging technique illustrated in Figure 2a, the position of threading dislocations in individual disks was recorded for 35 disks (13 disks with QW active regions and 22

DOI: 10.1021/ph500426g
ACS Photonics 2015, 2, 137–143

disks with QD active regions). Disks grown on lower defect material exhibit higher Q's, and those grown on high dislocation density material (5.3×10^9 cm^{-2}) have too low a quality to observe WGMs. The difference between the Q-factors of disks containing QWs and those containing QDs is statistically insignificant (t-test value $p = 0.44$) if made from samples of the same dislocation density. Figure 4 is a plot of the microdisk Q against the number of threading dislocations in specific regions of the disk. We can see that there is an anticorrelation observed between Q-factor and dislocation density when considering either the whole disk (Figure 4a) or just the outer region (Figure 4c). The correlation is stronger for TDs located in the outer region alone, although it should be noted that the size of etching residues caused by TDs (discussed later) is variable so that TDs that cause darks spots within the center region may still affect the outer modal region of the disk, smearing out this trend. There is no correlation of Q-factor with the dislocations located only in the inner region (Figure 4b). These correlations suggest that the dislocations, especially those located in the WGM region, play an important role in limiting quality factors. Thus, we believe that the dislocations play a more influential role on Q than the structure of the InGaN active layer itself (whether it is QW, fragmented QW, or QD).

The spatial resolution of CL, leading to the data displayed in Figure 4, allows us to focus our experiments and simulations to the regions of the microdisks where Q demonstrates the greatest sensitivity to dislocations. As stated earlier, the value of Q used in the plots of Figure 4 are the maximum Q of the disk, for any mode. Since the highest Q's pertain to the WGMs at the periphery of the disk, it is not surprising that the maximum Q is insensitive to dislocations in the center of the disk ($r < 0.4$ μm), where there is little overlap between the dislocation and the mode.

We investigate the mechanisms by which the presence of threading dislocations could negatively influence the microdisk Q; we first consider the existence of whiskers caused by the presence of dislocations. FDTD simulations of a microdisk cavity with a pyramidal whisker with a range of sizes (height of 150 nm, base widths of 100, 150, and 200 nm) located on the underside of the cavity membrane have been performed, in which the position of the whisker has been varied, from the center toward the edge of the disk. The simulation results suggest that the whisker creates a radiative pathway for light escape and show that the Q-factor of a first-order WGM decreases as the whisker approaches the edge of the microdisk cavity, where the mode is confined. Furthermore, the azimuthal position of the pyramid affects the degree to which the Q decreases: the Q value decreases more if the whisker is centered at the WGM antinode (i.e., high optical intensity) as opposed to on the node. Larger whiskers cause a larger effect. Figure 5 summarizes the results of the FDTD simulations. Such simulations corroborate our experimental observations that defects located in the high-field regions at the edge of the disk can be responsible for lowering the Q. Furthermore, the magnitude of Q-factor decrease we observe experimentally can be explained by the formation of even small whiskers, if located within the WGM volume.

It is also possible for TDs to increase the impurity level, both into the dislocation cores and in regions affected by the strain fields around the dislocation, and hence have an increased absorption coefficient relative to bulk GaN. While the strain fields associated with TDs can extend over a >10 nm scale, significant increases in doping occur over a scale of a few

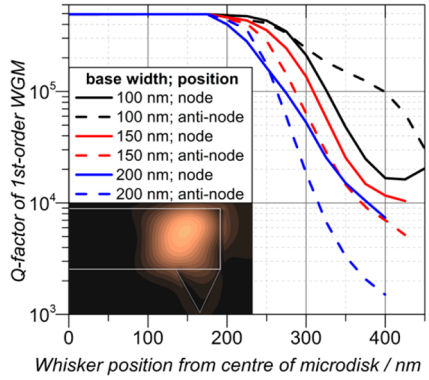

Figure 5. Q vs radial position of a pyramidal defect for three sizes of whisker (with a height of 150 nm and base widths of 100, 150, and 200 nm). Each size has a plot value for azimuthal position corresponding to a node and another for positioning on an antinode. (Inset) Side view of the field profile for a pyramid located at the edge of the disk (r = 375 nm) centered on the antinode of a first-order WGM. Light leaks into the whisker region and is subsequently radiated, lowering the Q.

nanometers.[26] FDTD simulations were performed in which dislocations were modeled as a 4 nm radius region of higher optical absorption, with a linear attenuation coefficient α. No significant effect was observed on cavity Q for values of α up to 10^9 cm^{-1}, which is many orders of magnitude greater than that expected for highly doped GaN ($\alpha < 10^4$ cm^{-1}),[27] and as such, we conclude that the small size of the dislocation removes any significant effect its optical absorption may have on the cavity Q.

It should be noted that TDs cause other effects, such as causing a shift in the absorption edge of bulk material through strain, having their own energy levels associated with defect and vacancy states at the TD core, and acting as nonradiative recombination centers.[28,29] However, the magnitude of the shift in optical absorption spectra relative to the bulk is largely insignificant,[30] and the energy levels associated with TD cores are outside the wavelength range used in these cavities.[31,32] The whiskers formed during PEC etching confirm the role of TDs as carrier traps and, thus, nonradiative recombination centers. Therefore, while they do directly affect internal quantum efficiency, they do not lead to a loss of photons and hence do not affect cavity quality factor. Our conclusion is that the limitations to Q posed by the TDs is through the whiskers formed during PEC etching, rather than any inherent property of the TDs themselves.

LIMITATIONS OF THE GAN SYSTEM

While we observe an anticorrelation between Q-factor and dislocation counts in the modal volume, we also see an upper limit of Q-factors for these cavities. Subsequent Q-measurements on dislocation-free cavities grown on samples with substrates fabricated using epitaxial lateral overgrowth give a Q-factor of 4800 ± 600, supporting this limit. For future application to cQED, such as strong coupling, the causes of this limit must be understood. The quality factor of a cavity may be described by eq 1.

$$Q^{-1} = Q_{ia}^{-1} + Q_r^{-1} + Q_{scat}^{-1} \quad (1)$$

where Q_{ia} denotes internal absorption losses, Q_r denotes intrinsic radiative losses, and Q_{scat} denotes surface scattering losses.

DOI: 10.1021/ph500426g
ACS Photonics 2015, 2, 137−143

Intrinsic radiative losses are determined by cavity design, decreasing with increasing disk radius.[33] In this regard, it is important to note that the highest value of Q is not necessarily the ultimate goal of the cavity design: the quality factor of the cavity should serve to facilitate the ultimate device application. For example, low-threshold laser designs typically use smaller cavities to increase the spontaneous emission factor and will, therefore, have greater intrinsic radiative loss.[34] While Q_r can be easily increased by changes in cavity design, this would be counterproductive to the intended purpose of the cavity, and it would not affect the total quality factor, as it is orders of magnitude bigger than the other values. The value of Q_r can be approximated as described in eq 2.[35,36]

$$Q_r \approx \exp(2MJ) \tag{2}$$

where M is the azimuthal mode number, $J = \tanh^{-1}(s) - s$, $s = (1 - (1/n^2))^{1/2}$, and n is the refractive index.

For our microdisks emitting at the observed wavelengths, this gives a value of Q_r of $\sim 3 \times 10^6$. FDTD simulations of such cavities with low absorption constants give a value of $Q = 8 \times 10^5$ (Figure 6). The difference between these analytical and computed values is explained by the approximations made in the simulation including loss from horizontal surfaces and meshing errors.

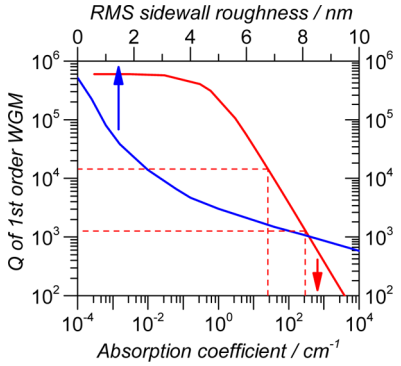

Figure 6. (Blue trace) Simulated Q of a WGM at 420 nm vs RMS roughness at the periphery of a 1 μm GaN microdisk. (Red trace) Q vs absorption coefficient, in which the disks are modeled as having no surface roughness. (Dashed line) Outer limits of absorption coefficients for GaN from literature and corresponding cavity Q-factors.[40,41]

Surface scattering depends on both disk morphology and surface roughness developed during fabrication, which in turn depend not only on etching conditions but also on the quality of etch mask used. AFM measurements of sidewall roughnesses in similar cavities have given values of approximately 2 nm.[37] The plasma-based (inductively coupled plasma) etch process used in the formation of the microdisks is well capable of creating <2 nm surfaces,[38] should the mask be adequately smooth. Our cavities were produced using silica masks with <0.2 nm surface roughness, and as such, we believe that our cavities should be similarly smooth, although AFM measurements of the sidewalls have not been performed. It should be additionally noted that samples previously produced by our group using the same methods have shown a measurable increase in sidewall roughness identifiable in SEM with no negative effect on cavity Q, and as such, we believe that the roughness is low enough not to limit cavity Q-factors. FDTD simulations were performed with a range of edge-wall roughnesses, with sidewall geometries modeled on those typically observed in fabricated devices as taken from SEM images: the correlation length in the radial and vertical dimensions is 30 and 300 nm, respectively. The relation of edge roughness to simulated Q_{scat} is given in Figure 6, in which no absorption effects were included in the simulation and the top horizontal surfaces of the disk were assumed to be smooth.

Q_{abs} can be approximated by eq 3.[39]

$$Q_{abs} = \frac{2\pi n_{eff}}{\alpha\lambda} \tag{3}$$

where α is the attenuation coefficient, n_{eff} is the effective refractive index of the medium, and λ is the wavelength of the mode considered. Internal absorption can be significant in the nitrides for emission below the band-edge of GaN due to moderate unintentional doping, leading to increased electronic transitions between donor−acceptor levels and structural defects.[27] For the wavelength of modes observed at 460 ± 14 nm, absorption coefficients have been stated in the range 30−350 cm^{-1} depending on growth conditions, dopant levels, and the substrate used,[27,40−42] leading to approximate Q_{abs} values between 10^3 and 10^4. Such a wide range may be explained by the variation in dopants and structural defects between the samples in these studies, leading to a wide variety of absorption in both the Urbach tail and free carrier absorption regions.[27] It is also possible, given the mode's location at the edge of the cavity, that there is a small contribution to the absorption coefficient from surface-state absorption. As such, the extinction coefficient used here represents an effective value that includes this component.

It should be noted for comparison that similar structures in other materials systems have achieved significantly higher Q-factors: $\sim 5 \times 10^5$ and $\sim 10^5$ for silicon and GaAs,[43,44] where the absorption coefficients are $\sim 10^{-4}$ and 1 cm^{-1}, respectively.[45,46] Q-factors in these devices are limited by intrinsic radiative and scattering losses, rather than absorption losses.

To further consider the limitations from internal absorption, the cavity structures were simulated with a range of absorption coefficients. We can see in Figure 6 not only the relationship between the absorption coefficient and cavity Q but also the point at which the internal absorption of the cavity becomes insignificant; for coefficients less than 1 cm^{-1} the intrinsic radiative loss of the cavity dominates the absorption loss and, hence, sets the limit of Q for cavities of these dimensions at $\sim 10^6$. Using previously stated values for the absorption coefficient of MOCVD-grown GaN gives the simulated Q_{abs} between 10^3 and 10^4, in agreement with calculated values. We can therefore use the simulations and measurements of Q to examine the limitations of the nitride cavities and the limitations of the nitride material system itself.

While scattering losses may be reduced by refinement of the plasma etching technique, the absorption losses pose a more difficult challenge to increasing nitride cavity Q-factor. Slight reduction of the free carrier absorption may be achievable by alteration of material growth conditions, although the sub-band-gap absorption in the wavelength range used for this study is significant at all achievable dopant levels.[27] It may therefore be more tractable to alter the wavelength of emission from the InGaN active layers to a lower energy, where the GaN absorption would be reduced. However, if emitters in the blue-green spectral region are desired, then only small decreases in absorption may be achieved; using the growth technique applied here it is difficult to produce high-quality InGaN QWs

DOI: 10.1021/ph500426g
ACS Photonics 2015, 2, 137−143

and QDs emitting at substantially lower energy in order to achieve a significant decrease in absorption.

To conclude, we have shown that we can identify the position of individual TDs in microcavities using CL. Using this method to map dislocation position across microdisks with a range of active layers, we observed an anticorrelation of the number of dislocations in a specific cavity with the cavity *Q*-factor. Simulations and SEM-CL spectra confirm that, as expected, the whispering gallery modes exist in the periphery of the microdisk cavities, and it is the dislocations in this region specifically that affect cavity *Q*. We suggest that the presence of TDs does not inherently cause a significant reduction in the *Q*-factor of the microcavities, but that they do cause the formation of unetched material during PEC etching, which subsequently causes optical leakage from the cavity. This loss may be avoided by using alternative fabrication methods. The limitations of the GaN system have been investigated, and internal absorption has been shown to be the significant factor in limiting cavity *Q*.

Overall, in our investigation we have shown that it is practicable to directly map materials defects and inhomogeneities in a fabricated microdevice. Our study exploited the resolution afforded by SEM-CL, allowing us to identify dislocations and their impact on the local electrical and optical properties within the cavities, and also cross-correlation with μPL to precisely measure the quality factor and hence quantify the optical loss. By combining these two techniques across a statistically significant number of devices, we are able to directly link specific defect-related features to device performance and to provide insights that could not be achieved by the more usual approach of assessing the general defect structure of the material from which devices are made. This approach, in which for a specific microdevice materials properties are mapped at high resolution and linked directly to measurements of device performance, should be broadly applicable to other semiconductor micro- and nanodevices, which will become increasingly important as other new and developing materials systems with defects and inhomogeneities are applied in photonics. This approach could certainly also utilize other microscopy techniques.

EXPERIMENTAL DETAILS

μPL measurements were made using a pulsed frequency-doubled Titanium-Sapphire laser emitting at 380 nm (76 MHz repetition rate, 200 fs pulse duration) through a high (0.90) numerical aperture (N.A.) objective normal to the surface of the microdisk. We estimate the pump laser spot size to be 0.4 μm^2. The collection path was through the same objective, and a long pass filter was placed before the spectrometer to remove any signal from the pump laser. All μPL measurements were performed at room temperature, with almost all (>95%) measured disks demonstrating whispering gallery modes superimposed over the inhomogeneously broadened QD or QW emission. CL measurements were obtained with a Philips XL30 SEM equipped with a Gatan MonoCL4 using a low accelerating voltage (3 kV, spot size 1, beam current 250 pA) and operating at room temperature, with the exception of the data in Figure 3, which were obtained on an Attolight CL system at 3 kV and a temperature of 15 K.[47]

AUTHOR INFORMATION

Corresponding Author

*(T. J. Puchtler) E-mail: tjp39@cam.ac.uk. Tel: +44 (0)1223 767930. Fax: +44 (0)1223 334437.

Author Contributions

T.J.P., A.W., T.Z., E.L.H., and R.A.O. designed the experiments; T.J.P., A.W., T.Z., and D.G. performed research; T.J.P., A.W., T.Z., E.L.H., and R.A.O. analyzed data and wrote the paper.

Notes

The authors declare no competing financial interest.

ACKNOWLEDGMENTS

This work has been funded in part by the EPSRC (Grant Nos. EP/H047816/1 and EP/G037221/1) and by the NSF Materials World Network (Award No. 1008480). This work was enabled by facilities available at the Center for Nanoscale Systems, a member of the National Nanotechnology Infrastructure Network (NNIN), which is supported by the National Science Foundation under NSF Award No. ECS-0335765. The European Research Council has provided financial support under the European Community's Seventh Framework Programme (FP7/2007-2013)/ERC grant agreement no. 279361 (MACONS). We thank the Attolight Company for use of their facilities.

REFERENCES

(1) Aleksiejūnas, R.; Sūdžius, M.; Malinauskas, T.; Vaitkus, J.; Jarašiūnas, K.; Sakai, S. Determination of Free Carrier Bipolar Diffusion Coefficient and Surface Recombination Velocity of Undoped GaN Epilayers. *Appl. Phys. Lett.* **2003**, *83*, 1157−1159.

(2) Muth, J. F.; Lee, J. H.; Shmagin, I. K.; Kolbas, R. M.; Casey, H. C.; Keller, B. P.; Mishra, U. K.; DenBaars, S. P. Absorption Coefficient, Energy Gap, Exciton Binding Energy, and Recombination Lifetime of GaN Obtained from Transmission Measurements. *Appl. Phys. Lett.* **1997**, *71*, 2572.

(3) Ramvall, P.; Tanaka, S.; Nomura, S.; Riblet, P.; Aoyagi, Y. Observation of Confinement-Dependent Exciton Binding Energy of GaN Quantum Dots. *Appl. Phys. Lett.* **1998**, *73*, 1104.

(4) Someya, T.; Werner, R.; Forchel, A.; Catalano, M.; Cingolani, R.; Arakawa, Y. Room Temperature Lasing at Blue Wavelengths in Gallium Nitride Microcavities. *Science* **1999**, *285*, 1905−1906.

(5) Tawara, T.; Gotoh, H.; Akasaka, T.; Kobayashi, N.; Saitoh, T. Cavity Polaritons in InGaN Microcavities at Room Temperature. *Phys. Rev. Lett.* **2004**, *92*, 256402.

(6) Aharonovich, I.; Woolf, A.; Russell, K. J.; Zhu, T.; Niu, N.; Kappers, M. J.; Oliver, R. A.; Hu, E. L. Low Threshold, Room-Temperature Microdisk Lasers in the Blue Spectral Range. *Appl. Phys. Lett.* **2013**, *103*, 021112.

(7) Reid, B. P. L.; Kocher, C.; Zhu, T.; Oehler, F.; Emery, R.; Chan, C. C. S.; Oliver, R. A.; Taylor, R. A. Observations of Rabi Oscillations in a Non-Polar InGaN Quantum Dot. *Appl. Phys. Lett.* **2014**, *104*, 263108.

(8) Jarjour, A. F.; Taylor, R. A.; Oliver, R. A.; Kappers, M. J.; Humphreys, C. J.; Tahraoui, A. Cavity-Enhanced Blue Single-Photon Emission from a Single InGaN/GaN Quantum Dot. *Appl. Phys. Lett.* **2007**, *91*, 052101.

(9) Mexis, M.; Sergent, S.; Guillet, T.; Brimont, C.; Bretagnon, T.; Gil, B.; Semond, F.; Leroux, M.; Néel, D.; David, S.; et al. High Quality Factor Nitride-Based Optical Cavities: Microdisks with Embedded GaN/Al(Ga)N Quantum Dots. *Opt. Lett.* **2011**, *36*, 2203−2205.

(10) Guillet, T.; Mexis, M.; Sergent, S.; Néel, D.; Rennesson, S.; Brimont, C.; Bretagnon, T.; Gil, B.; Sam-Giao, D.; Gayral, B.; et al. High Quality Factor Photonic Resonators for Nitride Quantum Dots. *Phys. Status Solidi* **2012**, *249*, 449−454.

(11) Sergent, S.; Arita, M.; Kako, S.; Iwamoto, S.; Arakawa, Y. High-*Q* (>5000) AlN Nanobeam Photonic Crystal Cavity Embedding GaN Quantum Dots. *Appl. Phys. Lett.* **2012**, *100*, 121103.

(12) Wang, Y.-S.; Chen, N.-C.; Lu, C.-Y.; Chen, J.-F. Optical Joint Density of States in InGaN/GaN-Based Multiple-Quantum-Well

DOI: 10.1021/ph500426g
ACS Photonics 2015, 2, 137−143

Light-Emitting Diodes. *Phys. B Condens. Matter* **2011**, *406*, 4300−4303.
(13) Tamboli, A. C.; Haberer, E. D.; Sharma, R.; Lee, K. H.; Nakamura, S.; Hu, E. L. Room-Temperature Continuous-Wave Lasing in GaN/InGaN Microdisks. *Nat. Photonics* **2007**, *1*, 61−64.
(14) Bernardini, F.; Fiorentini, V.; Vanderbilt, D. Spontaneous Polarization and Piezoelectric Constants of III-V Nitrides. *Phys. Rev. B* **1997**, *56*, R10024−R10027.
(15) Oliver, R. A.; Bennett, S. E.; Zhu, T.; Beesley, D. J.; Kappers, M. J.; Saxey, D. W.; Cerezo, A.; Humphreys, C. J. Microstructural Origins of Localization in InGaN Quantum Wells. *J. Phys. D. Appl. Phys.* **2010**, *43*, 354003.
(16) El-Ella, H. A. R.; Rol, F.; Kappers, M. J.; Russell, K. J.; Hu, E. L.; Oliver, R. A. Dislocation Density-Dependent Quality Factors in InGaN Quantum Dot Containing Microdisks. *Appl. Phys. Lett.* **2011**, *98*, 131909.
(17) Oliver, R. A.; Kappers, M. J.; Sumner, J.; Datta, R.; Humphreys, C. J. Highlighting Threading Dislocations in MOVPE-Grown GaN Using an in Situ Treatment with SiH_4 and NH_3. *J. Cryst. Growth* **2006**, *289*, 506−514.
(18) Stonas, A. R.; Kozodoy, P.; Marchand, H.; Fini, P.; DenBaars, S. P.; Mishra, U. K.; Hu, E. L. Backside-Illuminated Photoelectrochemical Etching for the Fabrication of Deeply Undercut GaN Structures. *Appl. Phys. Lett.* **2000**, *77*, 2610−2612.
(19) Haberer, E. D.; Sharma, R.; Meier, C.; Stonas, A. R.; Nakamura, S.; DenBaars, S. P.; Hu, E. L. Free-Standing, Optically Pumped, GaN/InGaN Microdisk Lasers Fabricated by Photoelectrochemical Etching. *Appl. Phys. Lett.* **2004**, *85*, 5179−5181.
(20) Oliver, R. A.; Briggs, G. A. D.; Kappers, M. J.; Humphreys, C. J.; Yasin, S.; Rice, J. H.; Smith, J. D.; Taylor, R. A. InGaN Quantum Dots Grown by Metalorganic Vapor Phase Epitaxy Employing a Post-Growth Nitrogen Anneal. *Appl. Phys. Lett.* **2003**, *83*, 755−757.
(21) Zhu, T.; El-Ella, H. A. R.; Reid, B.; Holmes, M. J.; Taylor, R. A.; Kappers, M. J.; Oliver, R. A. Growth and Optical Characterisation of Multilayers of InGaN Quantum Dots. *J. Cryst. Growth* **2012**, *338*, 262−266.
(22) Woolf, A.; Puchtler, T. J.; Aharonovich, I.; Zhu, T.; Niu, N.; Wang, D.; Oliver, R. A.; Hu, E. L. Distinctive Signature of Indium Gallium Nitride Quantum Dot Lasing in Microdisk Cavities. *Proc. Natl. Acad. Sci. U.S.A.* **2014**, *111*, 14042−14046.
(23) Khoury, M.; Courville, A.; Poulet, B.; Teisseire, M.; Beraudo, E.; Rashid, M. J.; Frayssinet, E.; Damilano, B.; Semond, F.; Tottereau, O.; et al. Imaging and Counting Threading Dislocations in c-Oriented Epitaxial GaN Layers. *Semicond. Sci. Technol.* **2013**, *28*, 035006.
(24) El-Ella, H. A. R.; Rol, F.; Collins, D. P.; Kappers, M. J.; Taylor, R. A.; Hu, E. L.; Oliver, R. A. InGaN Super-Lattice Growth for Fabrication of Quantum Dot Containing Microdisks. *J. Cryst. Growth* **2011**, *321*, 113−119.
(25) Weimann, N. G.; Eastman, L. F.; Doppalapudi, D.; Ng, H. M.; Moustakas, T. D. Scattering of Electrons at Threading Dislocations in GaN. *J. Appl. Phys.* **1998**, *83*, 3656−3659.
(26) Rhode, S. K.; Horton, M. K.; Kappers, M. J.; Zhang, S.; Humphreys, C. J.; Dusane, R. O.; Sahonta, S.-L.; Moram, M. A. Mg Doping Affects Dislocation Core Structures in GaN. *Phys. Rev. Lett.* **2013**, *111*, 025502.
(27) Ambacher, O.; Rieger, W.; Ansmann, P.; Angerer, H.; Moustakas, T. D.; Stutzmann, M. Sub-Bandgap Absorption of Gallium Nitride Determined by Photothermal Deflection Spectroscopy. *Solid State Commun.* **1996**, *97*, 365−370.
(28) Hino, T.; Tomiya, S.; Miyajima, T.; Yanashima, K.; Hashimoto, S.; Ikeda, M. Characterization of Threading Dislocations in GaN Epitaxial Layers. *Appl. Phys. Lett.* **2000**, *76*, 3421−3423.
(29) Miyajima, T.; Hino, T.; Tomiya, S.; Satake, A.; Tokunga, E.; Masumoto, Y.; Maruyama, T.; Ikeda, M. Non-Radiative Nature of Threading Dislocations in GaN Grown by Metalorganic Chemical Vapor Deposition. In *Proceedings of the International Workshop on Nitride Semiconductors*; IPAP Conf. Series 1, 2000; pp 536−539.
(30) Hasegawa, H.; Kamimura, Y.; Edagawa, K.; Yonenaga, I. Dislocation-Related Optical Absorption in Plastically Deformed GaN. *J. Appl. Phys.* **2007**, *102*, 026103.
(31) Elsner, J.; Jones, R.; Heggie, M.; Sitch, P.; Haugk, M.; Frauenheim, T.; Öberg, S.; Briddon, P. Deep Acceptors Trapped at Threading-Edge Dislocations in GaN. *Phys. Rev. B* **1998**, *58*, 12571−12574.
(32) Xin, Y.; James, E. M.; Arslan, I.; Sivananthan, S.; Browning, N. D.; Pennycook, S. J.; Omnès, F.; Beaumont, B.; Faurie, J. P.; Gibart, P. Direct Experimental Observation of the Local Electronic Structure at Threading Dislocations in Metalorganic Vapor Phase Epitaxy Grown Wurtzite GaN Thin Films. *Appl. Phys. Lett.* **2000**, *76*, 466−468.
(33) Borselli, M.; Johnson, T.; Painter, O. Beyond the Rayleigh Scattering Limit in High-Q Silicon Microdisks: Theory and Experiment. *Opt. Express* **2005**, *13*, 1515−1530.
(34) Chin, M. K.; Chu, D. Y.; Ho, S.-T. Estimation of the Spontaneous Emission Factor for Microdisk Lasers via the Approximation of Whispering Gallery Modes. *J. Appl. Phys.* **1994**, *75*, 3302−3307.
(35) McCall, S. L.; Levi, A. F. J.; Slusher, R. E.; Pearton, S. J.; Logan, R. A. Whispering-Gallery Mode Microdisk Lasers. *Appl. Phys. Lett.* **1992**, *60*, 289−291.
(36) Slusher, R. E.; Levi, A. F. J.; Mohideen, U.; McCall, S. L.; Pearton, S. J.; Logan, R. A. Threshold Characteristics of Semiconductor Microdisk Lasers. *Appl. Phys. Lett.* **1993**, *63*, 1310−1312.
(37) Lee, J.-S.; Lee, J.; Kim, S.; Jeon, H. Fabrication of Reflective GaN Mesa Sidewalls for the Application to High Extraction Efficiency LEDs. *Phys. Status Solidi* **2007**, *4*, 2625−2628.
(38) Shul, R. J.; Zhang, L.; Baca, A. G.; Willison, C. G.; Han, J.; Pearton, S. J.; Ren, F. Inductively Coupled Plasma-Induced Etch Damage of GaN P-N Junctions. *J. Vac. Sci. Technol., A* **2000**, *18*, 1139−1143.
(39) Simeonov, D.; Feltin, E.; Bühlmann, H.-J.; Zhu, T.; Castiglia, A.; Mosca, M.; Carlin, J.-F.; Butté, R.; Grandjean, N. Blue Lasing at Room Temperature in High Quality Factor GaN/AlInN Microdisks with InGaN Quantum Wells. *Appl. Phys. Lett.* **2007**, *90*, 061106.
(40) Omnès, F.; Marenco, N.; Beaumont, B.; de Mierry, P.; Monroy, E.; Calle, F.; Muñoz, E. Metalorganic Vapor-Phase Epitaxy-Grown AlGaN Materials for Visible-Blind Ultraviolet Photodetector Applications. *J. Appl. Phys.* **1999**, *86*, 5286.
(41) Strite, S.; Morkoç, H. GaN, AlN, and InN: A Review. *J. Vac. Sci. Technol., B* **1992**, *10*, 1237.
(42) Yu, G.; Wang, G.; Ishikawa, H.; Umeno, M.; Soga, T.; Egawa, T.; Watanabe, J.; Jimbo, T. Optical Properties of Wurtzite Structure GaN on Sapphire around Fundamental Absorption Edge (0.78−4.77 eV) by Spectroscopic Ellipsometry and the Optical Transmission Method. *Appl. Phys. Lett.* **1997**, *70*, 3209−3211.
(43) Borselli, M.; Srinivasan, K.; Barclay, P. E.; Painter, O. Rayleigh Scattering, Mode Coupling, and Optical Loss in Silicon Microdisks. *Appl. Phys. Lett.* **2004**, *85*, 3693−3695.
(44) Srinivasan, K.; Painter, O. Linear and Nonlinear Optical Spectroscopy of a Strongly-Coupled Microdisk-Quantum Dot System. *Nat. Lett.* **2007**, *450*, 862−866.
(45) Green, M. A. Self-Consistent Optical Parameters of Intrinsic Silicon at 300K Including Temperature Coefficients. *Sol. Energy Mater. Sol. Cells* **2008**, *92*, 1305−1310.
(46) Sturge, M. D. Optical Absorption of Gallium Arsenide between 0.6 and 2.75 eV. *Phys. Rev.* **1962**, *127*, 768−773.
(47) Zhang, Q.; Lee, Y. H.; Phang, I. Y.; Pedireddy, S.; Tjiu, W. W.; Ling, X. Y. Bimetallic Platonic Janus Nanocrystals. *Langmuir* **2013**, *29*, 12844−12851.

DOI: 10.1021/ph500426g
ACS Photonics 2015, 2, 137−143